MOLECULAR AND CELLULAR BIOLOGY, July 2010, p. 3553–3568 Vol. 30, No. 14
0270-7306/10/$12.00 doi:10.1128/MCB.01445-09

Nox4-Derived H_2O_2 Mediates Endoplasmic Reticulum Signaling through Local Ras Activation[▽]

Ru-Feng Wu, Zhenyi Ma, Zhe Liu, and Lance S. Terada*

Department of Internal Medicine, Division of Pulmonary and Critical Care, University of Texas Southwestern Medical Center, 5323 Harry Hines Boulevard, Dallas, Texas 75390

Received 3 November 2009/Returned for modification 27 December 2009/Accepted 2 May 2010

The unfolded-protein response (UPR) of the endoplasmic reticulum (ER) has been linked to oxidant production, although the molecular details and functional significance of this linkage are poorly understood. Using a ratiometric H_2O_2 sensor targeted to different subcellular compartments, we demonstrate specific production of H_2O_2 by the ER in response to the stressors tunicamycin and HIV-1 Tat, but not to thapsigargin or dithiothreitol. Knockdown of the oxidase Nox4, expressed on ER endomembranes, or expression of ER-targeted catalase blocked ER H_2O_2 production by tunicamycin and Tat and prevented the UPR following exposure to these two agonists, but not to thapsigargin or dithiothreitol. Tat also triggered Nox4-dependent, sustained activation of Ras leading to ERK, but not phosphatidylinositol 3-kinase (PI3K)/mTOR, pathway activation. Cell fractionation studies and green fluorescent protein (GFP) fusions of GTPase effector binding domains confirmed selective activation of endogenous RhoA and Ras on the ER surface, with ER-associated K-Ras acting upstream of the UPR and downstream of Nox4. Notably, the Nox4/Ras/ERK pathway induced autophagy, and suppression of autophagy unmasked cell death and prevented differentiation of endothelial cells in 3-dimensional matrix. We conclude that the ER surface provides a platform to spatially organize agonist-specific Nox4-dependent oxidative signaling events, leading to homeostatic protective mechanisms rather than oxidative stress.

Coupled in part to its function as a major site of protein synthesis, the endoplasmic reticulum (ER) has emerged as an important signaling organelle, responding to various cell stresses and controlling cell fate. Much of this signaling is initiated on the ER membrane surface. In response to an overload of misfolded client proteins in the ER lumen, for example, transmembrane ER stress sensors such as IRE1, PERK, and ATF6 initiate signals on the cytosolic face of the ER to reduce global protein synthesis, promote protein folding, and increase the degradation of misfolded proteins (36). Failure of this response to alleviate protein misfolding stress leads to late expression of proteins such as CHOP, culminating in cell death. In addition to factors controlling this unfolded-protein response (UPR), cyclins, pro- and anti-apoptotic BH3 domain proteins, caspases, and signaling adapters associate with the ER surface and control cell cycle entry, cell death, Ca^{2+} flux, amino acid metabolism, oxidative-stress response, and autophagy (15, 17–19, 41). Thus, the ER integrates a variety of stresses (metabolic, protein misfolding, and oxidative) to coordinate cellular stress responses.

Another ER transmembrane protein is the NADPH oxidase Nox4. Like other Nox family members, Nox4 produces H_2O_2 and is thought to function primarily in cell signaling. Consistent with its ER localization, Nox4 mediates oxidative inactivation of the ER-resident phosphatase PTP1B and responds to ER stress induced by the LDL oxysterol 7-ketocholesterol (10, 34). The presence of Nox4 on the ER surface is notable, since ER stress is associated with the production of reactive oxygen species (ROS), though the nature of this association is poorly understood. Agents that cause ER stress initiate ATF4-dependent glutathione (GSH) synthesis, which is necessary to diminish ROS production and subsequent cell death (15). The mechanism of ROS production is also unclear, but it is thought to be a consequence of the UPR, possibly downstream of CHOP (25, 26). For the most part, such studies suggest a role for oxidants as late effectors of cell death, downstream from the UPR. The ER itself may be a source of oxidants, as knockdown of the ER oxidase Ero-1 in *pek-1*-null worms diminishes oxidant production (15). To some extent, the excessive production of ROS by the stressed ER would seem to run counter to recent observations that chemical and physiologic ER stressors converge on the production of a hyperreduced ER interior (28). In addition, [*rho*^{0}] *Saccharomyces cerevisiae* lacking mitochondria also fails to produce ROS in response to ER stress, suggesting a mitochondrial source (16). In part, such studies linking the ER and oxidative stress have been hampered by reliance on probes, such as dichlorofluorescein, that are untargeted and nonspecific, reacting with a broad variety of oxidants as well as non-ROS compounds, such as cytosolic cytochrome *c*.

In this study, using an H_2O_2-specific probe targeted to the ER, we found that Nox4 participates early in ER stress signaling in an agonist-specific fashion through a novel process involving focal activation of Ras on the ER. This Nox4-dependent pathway leads to activation of autophagy, which prevents the progression of the UPR to cell death, thus distinguishing Nox4 oxidant signaling from oxidative stress.

MATERIALS AND METHODS

Plasmid, adenovirus, and lentivirus construction. Human Nox4 cDNA was obtained from Open Biosystems; NheI and SalI sites were added, and the open reading frame (ORF) was subcloned into the adenoviral shuttle vector pDC315io (Microbix) to generate pDC315-Nox4. Human p22^{phox} cDNA was also obtained

* Corresponding author. Mailing address: University of Texas Southwestern, 5323 Harry Hines Blvd., MC 8558, Dallas, TX 75390. Phone: (214) 648-9099. Fax: (214) 648-9104. E-mail: Lance.Terada@utsouthwestern.edu.

▽ Published ahead of print on 10 May 2010.

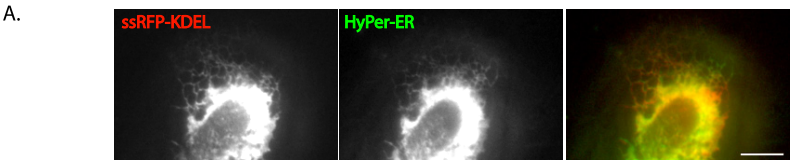
A.
ssRFP-KDEL
HyPer-ER

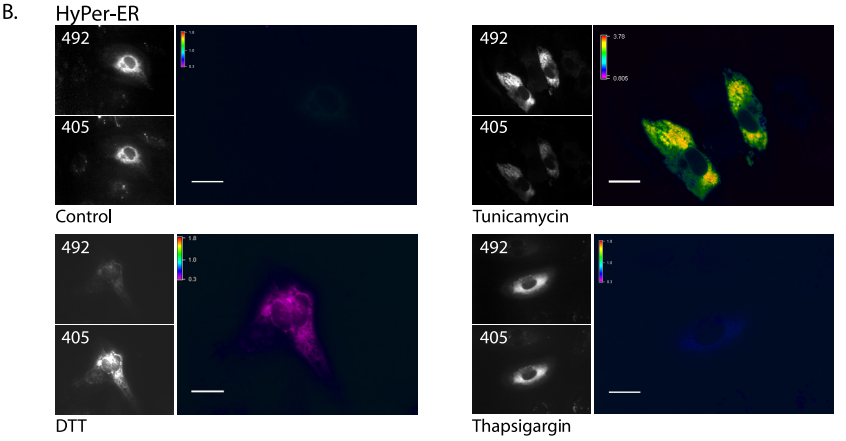
B.
HyPer-ER
492
405
Control
Tunicamycin
DTT
Thapsigargin

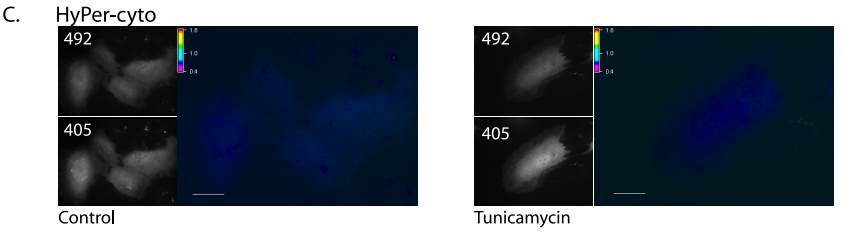
C.
HyPer-cyto
492
405
Control
Tunicamycin

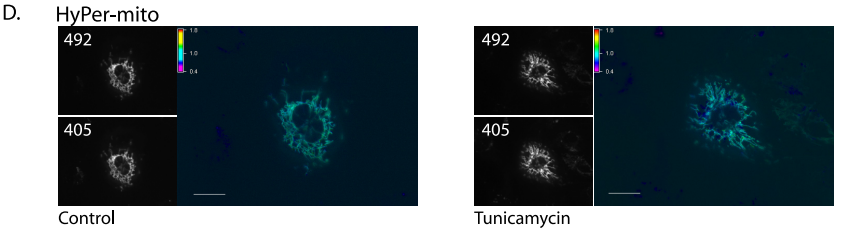
D.
HyPer-mito
492
405
Control
Tunicamycin

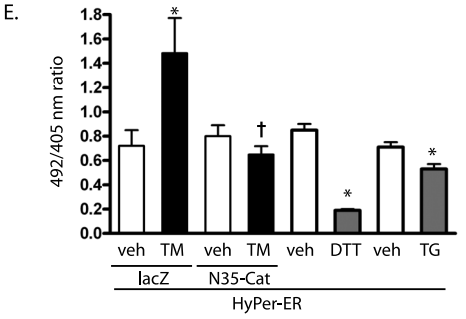
E.
492/405 nm ratio
1.8
1.6
1.4
1.2
1.0
0.8
0.6
0.4
0.2
0.0
veh TM veh TM veh DTT veh TG
lacZ
N35-Cat
HyPer-ER

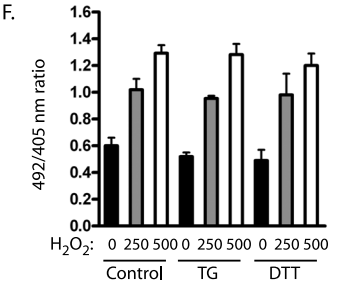
F.
492/405 nm ratio
1.6
1.4
1.2
1.0
0.8
0.6
0.4
0.2
0.0
H2O2: 0 250 500 0 250 500 0 250 500
Control
TG
DTT

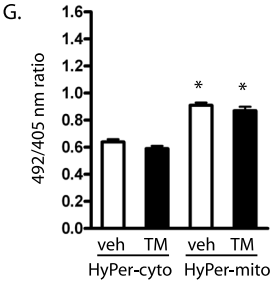
G.
492/405 nm ratio
1.6
1.4
1.2
1.0
0.8
0.6
0.4
0.2
0.0
veh TM veh TM
HyPer-cyto HyPer-mito

from Open Biosystems. After the addition of terminal EcoRI and SalI sites, the ORF was subcloned into the shuttle vector to create pDC315-p22. N35-Cat containing an N-terminal ER-targeting motif (obtained from Kai Chen) fused to catalase was released with NheI and SalI and inserted into the shuttle vector to create pDC315-N35-Cat. These plasmids were each cotransfected with the adenovirus (Ad) backbone pBHGlox(del)E1,3Cre into 293IQ packaging cells (Microbix). Viral plaques were cloned and expanded, and the titers were determined. The control adenovirus Ad-lacZ was described previously (43). Ad-RhoA(N19) was a gift of Christopher Chen.

Target sequences for human Nox2 (nucleotides [nt] 1291 to 1309), Nox4 (nt 409 to 427), K-Ras (nt 333 to 351), N-Ras (nt 351 to 369), and Atg5 (nt 589 to 607) were used to create oligonucleotides creating short hairpin RNA (shRNA) loops. Oligonucleotide pairs were first ligated into pSUPER.retro.puro (Oligoengine). Fragments containing the shRNA sequence and the H1 promoter were then excised and ligated into the lentiviral transfer construct pCCL.PPT.hPGK.GFP.Wpre (a gift from Phil Scherer) opened with either SalI/EcoRV or XhoI/EcoRV. The former restriction pair resulted in the insertion of the shRNA expression cassette and loss of green fluorescent protein (GFP), which was essential for HyPer studies.

Human Nox4 was ligated into pEGFP-N3 to create Nox4-GFP (C-term), in which GFP was fused to the C terminus of Nox4. Nox4 was also fused to the C terminus of GFP using pEGFP-C3 to create GFP-Nox4 (N-term). The untargeted ratiometric H_2O_2 sensor pHyPer-Cyto and the mitochondrially targeted probe pHyPer-mito were obtained from Evrogen. The signal sequence of bovine preprolactin, encoding the first 30 residues, was inserted upstream of HyPer into the NheI site, and an oligonucleotide encoding the ER retention signal KDEL/stop was inserted at the 3′ end of HyPer to create HyPer-ER. ssRFP-KDEL, ssGFP-KDEL, GFP-LC3, and RBD3(R59A)-GFP were gifts from Anil Agarwal, Eija Jokitalo, Beth Levine, and Ignacio Rubio, respectively. The RhoA-binding domain of rhotekin fused to GFP (RhBD-GFP) or glutathione *S*-transferase (GST) (RBD-GST) and the Ras binding domain (RBD) of Raf (Raf-GST) were previously described (24, 45). All new constructs were confirmed by sequencing.

Cell culture and other reagents. Human umbilical vein endothelial cells (HUVEC) were obtained from Clonetics; grown in EGM-2 medium containing 2% fetal calf serum, epidermal growth factor (EGF), fibroblast growth factor (FGF), vascular endothelial growth factor (VEGF), insulin-like growth factor, ascorbic acid, hydrocortisone, heparin, and gentamicin; and used at passage 4 or 5. HeLa-Tat cells, which secrete biologically active Tat (12, 14), were obtained from the AIDS Research and Reference Reagent Program (NIH). For coculture experiments, HeLa or HeLa-Tat cells were grown on the upper chamber of 0.4-μm-pore-size six-well transwell filters (Costar), with HUVEC plated on the bottom chamber.

Tunicamycin, thapsigargin, and dithiothreitol (DTT) were obtained from Sigma-Aldrich. Antibodies against Tat were obtained from the AIDS Research and Reference Reagent Program.

Immunoblotting. Blotting was performed for phospho-T981-PERK, phospho-JNK, phospho-T308-Akt (Santa Cruz), phospho-S51-eIF2α, phospho-ERK, phospho-T389-p70S6K, or phospho-S2448-mTOR (Cell Signaling). The blots were stripped and reprobed for total PERK, eIF2α, JNK, Akt (Santa Cruz), p70S6K (Cell Signaling), or mTOR (BioLegend). Other antibodies used were BiP, Nox2, and pan-Ras from BD; actin from Chemicon; and Nox4 (polyclonal H-300) and CHOP from Santa Cruz.

XBP-1 splicing. XBP-1 splicing was assessed as previously described (42). In brief, total RNA was extracted from HUVEC using TRIzol (Invitrogen), treated with DNase (Promega), extracted with phenol, and precipitated in ethanol. Oligo(dT) was used to prime the reverse transcription (RT) reaction, followed by PCR across the splice junction using the forward primer 5′-CCTTGTAGTTGAGAACCAGG-3′ and the reverse primer 5′-CAGAATGCCCAACAGGATATC-3′. The PCR products were restricted with PstI.

ER isolation. Five 100-mm dishes of HUVEC were pooled, washed twice with PBS, resuspended in 3 pellet volumes (~0.6 ml) of hypotonic extraction buffer (10 mM HEPES, pH 7.8, 25 mM KCl, 1 mM EGTA, protease inhibitor cocktail), and incubated for 20 min at 4°C to allow swelling. The 600 × *g* pellet was then resuspended in 2 pellet volumes (~0.2 ml) of isotonic extraction buffer (10 mM HEPES, pH 7.8, 250 mM sucrose, 25 mM KCl, and 1 mM EGTA) and homogenized with 10 passes through a 23-gauge needle, followed by 2 brief passes with a Potter-Elvehjem homogenizer at low speed (200 rpm). Optiprep (iodixanol; Sigma) was then added to a final concentration of 20%, and 0.75 ml of the homogenate was laid over 1 ml of 30% Optiprep. Two milliliters of 15% Optiprep was overlaid onto the homogenate, and the sample was centrifuged at 150,000 × *g* for 3 h at 4°C using a SW55Ti rotor. Fractions (0.25 ml) of the discontinuous gradient were acetone precipitated twice and resolved by SDS-PAGE. Immunoblots for HSP60 (Abcam), calregulin and Na-K ATPase (Santa Cruz), and BiP and caveolin 1 (BD) were performed to mark organellar content.

Transduction and knockdown. HUVEC were grown to 60 to 80% confluence prior to adenoviral or lentiviral transduction. For lentiviral transduction, Phoenix-293 cells were cotransfected with the transfer constructs and the third-generation packaging plasmids pMD2.VSVG, pMDLg/pRRE, and pRSV-REV, and fresh supernatant was used for infection. After 2 h (adenovirus) or 8 h (lentivirus) of infection, the HUVEC were washed and allowed to recover for 24 h prior to coculture with HeLa-Tat or HeLa cells.

GTPase activity. RhoA and Ras activation was assessed using a pulldown technique. RBD-GST and Raf-GST were expressed in *Escherichia coli* BL21-RP (Stratagene) and purified on GSH-Sepharose (GE Healthcare). HUVEC lysate was centrifuged at 10,000 × *g*; 2/3 of the supernatant was used for pulldown with the respective fusions and immunoblotted for RhoA (Santa Cruz) or pan-Ras (BD), while 1/3 of the lysate was precipitated in ice-cold acetone (1:1) for assessment of total GTPase.

Microscopy. The ventral surfaces of cells were imaged at high resolution using total internal reflection fluorescence (TIRF) microscopy. HUVEC were plated on 35-mm coverslip bottom dishes coated with fibronectin. For coculture experiments, Transwell inserts were placed into these dishes and HUVEC were examined during coculture. GFP and red fluorescent protein (RFP) chromophores were excited with 488-nm (argon) or 543-nm (HeNe) laser lines using TIRF optics through a 1.45-numeric-aperture (NA) oil immersion objective (Nikon) on a Nikon TE2000-U microscope in a 37°C heated chamber. Images were obtained with a charge-coupled device (CCD) camera (Coolsnap ES; Roper Scientific) using Metamorph software (Molecular Devices).

Imaging of H_2O_2 with HyPer was performed using 405/40 and 492/18 bandpass excitation and 530/35 bandpass emission filters (Chroma). Live-cell microscopy was performed at 37°C. Sequential 1.0-s unbinned exposures at each excitation peak were obtained without saturation and analyzed with NIS Elements AR3.0 software (Nikon). Whole-cell regions of interest were background subtracted and used to quantify HyPer ratios. Statistical analysis was performed using analysis of variance (ANOVA) with Tukey's posthoc intergroup comparison test.

Cell death. DNA fragmentation was assessed using a Cell Death enzyme-linked immunosorbent assay (ELISA) (Roche). Absorbance values were normalized to cell numbers.

Transmission electron microscopy. HUVEC were fixed *in situ* (2.5% glutaraldehyde, 0.1 M sodium cacodylate), harvested by scraping, and postfixed with osmium tetroxide prior to dehydration with graded ethanol into propylene oxide. Cell blocks were embedded in EMbed 812 (Electron Microscopy Sciences), sectioned, placed on copper grids, stained with uranyl acetate and lead citrate,

FIG. 1. Tunicamycin increases ER H_2O_2. (A) Cotransfection of HyPer-ER (green channel) and ssRFP-KDEL (red channel) shows colocalization. The image was acquired with TIRF optics. Scale bar, 10 μm. (B) HUVEC transfected with HyPer-ER were treated with vehicle (0.001% dimethyl sulfoxide [DMSO]), tunicamycin (10 μg/ml), DTT (2 mM), or thapsigargin (0.4 μM) for 16 h and sequentially excited at 492 and 405 nm. The grayscale images show the relative intensities of representative fields; 492/405 ratios are shown as pseudocolored images. Scale bars, 20 μm. (C and D) HUVEC transfected with untargeted HyPer-cyto (C) or mitochondrially targeted HyPer-mito (D) were treated with vehicle or tunicamycin for 16 h and ratio imaged. Scale bars, 20 μm. (E) 492/405 ratios were quantified for cells treated with corresponding vehicle (veh), tunicamycin (TM), DTT, or thapsigargin (TG). The indicated cells were exposed to adenovirus harboring *lacZ* (control) or ER-targeted catalase (N35-Cat). Means and standard errors of the mean (SEM) for 8 to 18 individual determinations are shown. *, $P < 0.05$ from vehicle. Expression of N35-Cat decreased the ratio of TM-treated cells (†, $P < 0.01$ from TM-plus-lacZ control). (F) HUVEC were transfected with HyPer-ER and exposed to thapsigargin or DTT for 16 h. The reagent H_2O_2 was added in the indicated concentrations, and 492/405 ratio images were taken after 3 to 5 min. (G) 492/405 ratios were quantified for cells transfected with either HyPer-cyto or HyPer-mito and treated with vehicle or tunicamycin for 16 h. Means and SEM of 12 to 15 individual determinations are shown. *, $P < 0.001$ from HyPer-cyto/vehicle.

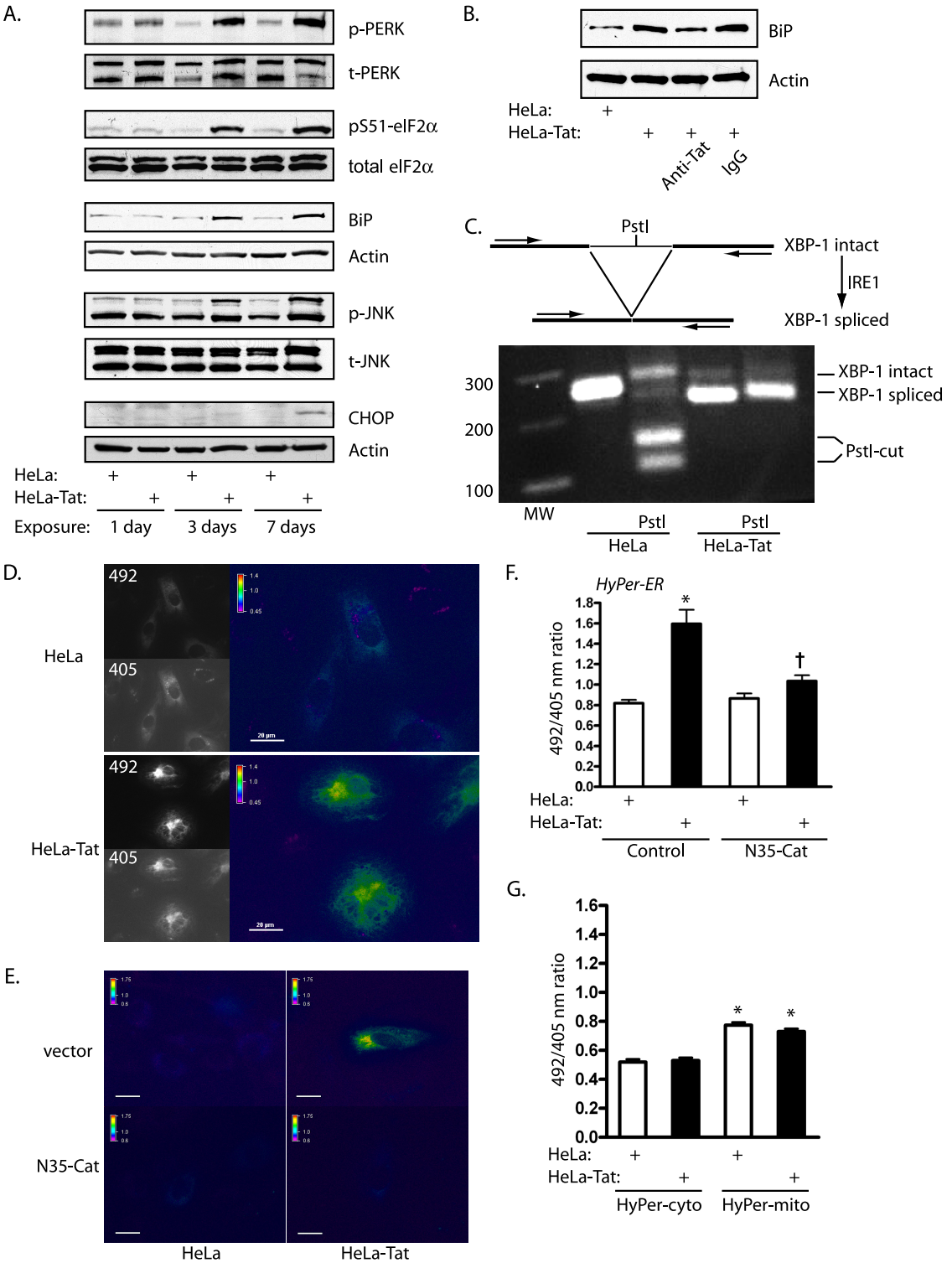

FIG. 2. HIV-1 Tat activates the UPR and increases ER H_2O_2 levels. (A) HUVEC were cocultured with HeLa or HeLa-Tat cells for 1, 3, or 7 days. The HeLa-Tat cells were removed, and the HUVEC were immunoblotted with the indicated antibodies. Phosphorylation of PERK, eIF2α, p-PERK, phospho-PERK; t-PERK, total PERK, and JNK and induction of BiP occurred at 3 and 7 days. CHOP was induced at 7 days. The blots are representative of 2 to 4 experiments. (B) HUVEC were cocultured with (+) HeLa or HeLa-Tat cells in the presence of anti-Tat antibodies (1:500) or control IgG (1:500) for 3 days and then immunoblotted for BiP. (C) (Top) cartoon showing splicing of XBP-1 transcript to a smaller transcript lacking an internal PstI site, with the positions of PCR primers. (Bottom) Ethidium bromide gel of RT-PCR products demonstrating reduction in PCR fragment size and loss of the PstI site. (D) HUVEC transfected with HyPer-ER were cocultured with HeLa or HeLa-Tat cells for 3 days and subjected to ratio imaging. (E) HUVEC cotransfected with empty vector or N35-Cat were exposed to HeLa or HeLa-Tat cells for 3 days. Representative pseudocolored ratio images are shown. Scale bars, 20 μm. (F) HyPer ratios were quantified from the conditions in panel E. The means plus SEM of 12 to 16 determinations are shown. ∗, $P < 0.001$ from control; †, $P < 0.001$ from HeLa-Tat with vector control. (G) HUVEC transfected with HyPer-cyto or HyPer-mito were cocultured with HeLa or HeLa-Tat cells for 3 days, and ratio images were quantified. The means plus SEM of 9 to 12 determinations are shown. ∗, $P < 0.001$ from HyPer-cyto/HeLa control.

and examined with an FIE Tecnai G2 Spirit Biotwin transmission electron microscope (TEM).

Matrigel tube assay. HUVEC were plated onto thick (1-mm) layers of Matrigel in six-well chambers and immediately exposed to HeLa or HeLa-Tat cells in Transwell inserts. Branching of tubular structures was assessed by random counts of at least five low-power fields per well.

RESULTS

H_2O_2 is selectively produced on the ER by tunicamycin and HIV-1 Tat. In order to visualize focal oxidant production by the ER, we employed HyPer, a recently described fluorescent sensor composed of circularly permuted yellow fluorescent protein (cpYFP) inserted into the regulatory domain of the H_2O_2-specific bacterial reporter OxyR (5). Oxidation of OxyR Cys199/208, which flank cpYFP, by submicromolar levels of H_2O_2 causes a reversible spectral shift in cpYFP, resulting in an increase in the 500-nm and a decrease in the 420-nm absorbance peaks. Thus, the probe acts as a ratiometric H_2O_2-specific sensor, with ratios independent of probe concentrations (5). We fused a leader sequence to the N terminus and the ER retention C-terminal KDEL motif to this sensor to target it to the ER. This probe (HyPer-ER) colocalized with ssRFP-KDEL, indicating proper ER targeting (Fig. 1A). Interestingly, despite the oxidizing environment of the ER, H_2O_2 levels were only minimally above background in control HUVEC (Fig. 1B). The 492/405 ratios of HyPer targeted to the ER were similar to the ratios of untargeted HyPer free in the cytosol under resting conditions (0.76 ± 0.03 cytosol, 0.82 ± 0.26 ER; $P > 0.05$). We then examined the response of ER H_2O_2 levels to the addition of three chemical compounds known to cause ER stress through different mechanisms: the glycosylation inhibitor tunicamycin, the ER Ca^{2+} reuptake inhibitor thapsigargin, and the reductant dithiothreitol (DTT). Tunicamycin caused an increase in ER H_2O_2 levels, whereas both thapsigargin and DTT decreased ER H_2O_2 (Fig. 1B and E). The lack of H_2O_2 signals from the last two agonists was not due to misfolding of HyPer-ER, as addition of H_2O_2 to cells pretreated with thapsigargin and DTT displayed increased 492/405 ratios from HyPer-ER, similar to those of control cells (Fig. 1F). To confirm that the increase in the HyPer ratio was due to H_2O_2, ER-targeted catalase (N35-Cat) (10) was expressed with HyPer-ER in HUVEC. N35-Cat blocked the tunicamycin-induced increase in HyPer ratios, confirming the oxidant produced to be H_2O_2 (Fig. 1E). HyPer was then targeted to the cytosol and to mitochondria to assess whether H_2O_2 production was ER specific. Whereas basal mitochondrial H_2O_2 levels were higher than cytosolic levels, H_2O_2 production did not increase in either of these compartments during tunicamycin-induced ER stress (Fig. 1C, D, and G). Thus, tunicamycin specifically increases H_2O_2 production by the ER.

We next studied a physiologically relevant agonist, HIV-1 Tat. This viral peptide causes ER stress when injected into mice *in vivo*, and the brains of HIV-infected humans display signs of ER stress and activation of the UPR (23, 29). We found that sustained exposure of HUVEC to Tat through coculture with Tat-secreting HeLa cells (HeLa-Tat) caused broad activation of the UPR by 3 days, with phosphorylation of PERK, eIF2α, and JNK and induction of Grp78/BiP (Fig. 2A). Coincubation with antibodies against Tat blocked BiP induction, confirming the specificity of the effects for Tat (Fig. 2B). In addition, nearly complete splicing of the XBP-1 transcript by the ER stress sensor IRE1 was detected by RT-PCR (Fig. 2C). HyPer-ER imaging demonstrated increased 492/405 ratios within 3 days of exposure to Tat, temporally correlating with UPR activation, and this increase was effectively blocked by ER-directed catalase, demonstrating an increase in ER H_2O_2 production by Tat (Fig. 2D to F). CHOP expression did not increase until 7 days, suggesting that oxidant production was not downstream of CHOP. As with tunicamycin, HyPer directed to the cytosol and to mitochondria indicated that H_2O_2 production stimulated by Tat was restricted to the ER (Fig. 2G).

Nox4-derived H_2O_2 mediates tunicamycin- and Tat-induced UPR. Endogenous and chromophore- or epitope-tagged Nox4 have been found associated with a number of subcellular compartments, but most consistently with ER membranes (10, 27, 34, 40). To image the ER at high resolution, TIRF microscopy was used to visualize ventral ER structures close to the plasma membrane. The conformation of the ER in this location takes on a characteristic reticular, branching tubular network, as opposed to ER sheets formed more dorsally (35). In live, unfixed, and unpermeabilized HUVEC, Nox4-GFP distribution replicated this reticular distribution as visualized by the ER marker ssGFP-KDEL (Fig. 3 A). In addition, GFP, when fused to Nox4 at either its C or N terminus, colocalized with the ER marker ssRFP-KDEL (Fig. 3B and C). Cell fractionation studies confirmed that endogenous Nox4 was recovered in iodixanol fractions containing the ER-resident proteins calregulin and BiP, but not markers for the plasma membrane or mitochondria (Fig. 3D). The molecular mobility of Nox4 in ER fractions was approximately 66.0 kDa, consistent with the predicted unmodified form of Nox4 (66.9 kDa). The contribution of Nox4 to early ER stress-induced H_2O_2 production was assessed through stable shRNA expression, accomplished with lentiviral transduction. Nox4 knockdown decreased both Tat- and tunicamycin-induced HyPer-ER ratios to baseline levels, implicating Nox4 as the primary source of H_2O_2 from the ER itself under stress (Fig. 3E to G). To confirm that Nox4 can increase ER H_2O_2 levels, we overexpressed Nox4 and its cognate subunit, $p22^{phox}$, and found that overexpression increased ER H_2O_2 levels comparably to tunicamycin, and the combination of Nox4 overexpression and tunicamycin increased ER H_2O_2 levels further (Fig. 3H).

Although ROS are best recognized as mediators of oxidative stress and consequent cell death, the Nox proteins frequently participate in homeostatic signaling through regulated and site-directed oxidant production (38). To investigate whether Nox4 participates in ER stress signaling, we studied the UPR following knockdown of Nox4 or Nox2, the predominant Nox members expressed by HUVEC. Lentiviral infection itself did not induce BiP, suggesting lack of effect of lentiviral transduction on ER stress. shRNA against Nox4 strongly suppressed phosphorylation of eIF2α and induction of BiP and CHOP by tunicamycin, whereas shRNA against Nox2 had no effect (Fig. 4A and B). In contrast, neither Nox4 nor Nox2 knockdown had measurable effects on these UPR events following exposure to thapsigargin or DTT, consistent with the lack of H_2O_2 production by the ER from these agonists (Fig. 4A). Accordingly, ER-targeted catalase completely blocked BiP induction by tunicamycin but had no effect on BiP induction by thapsigargin

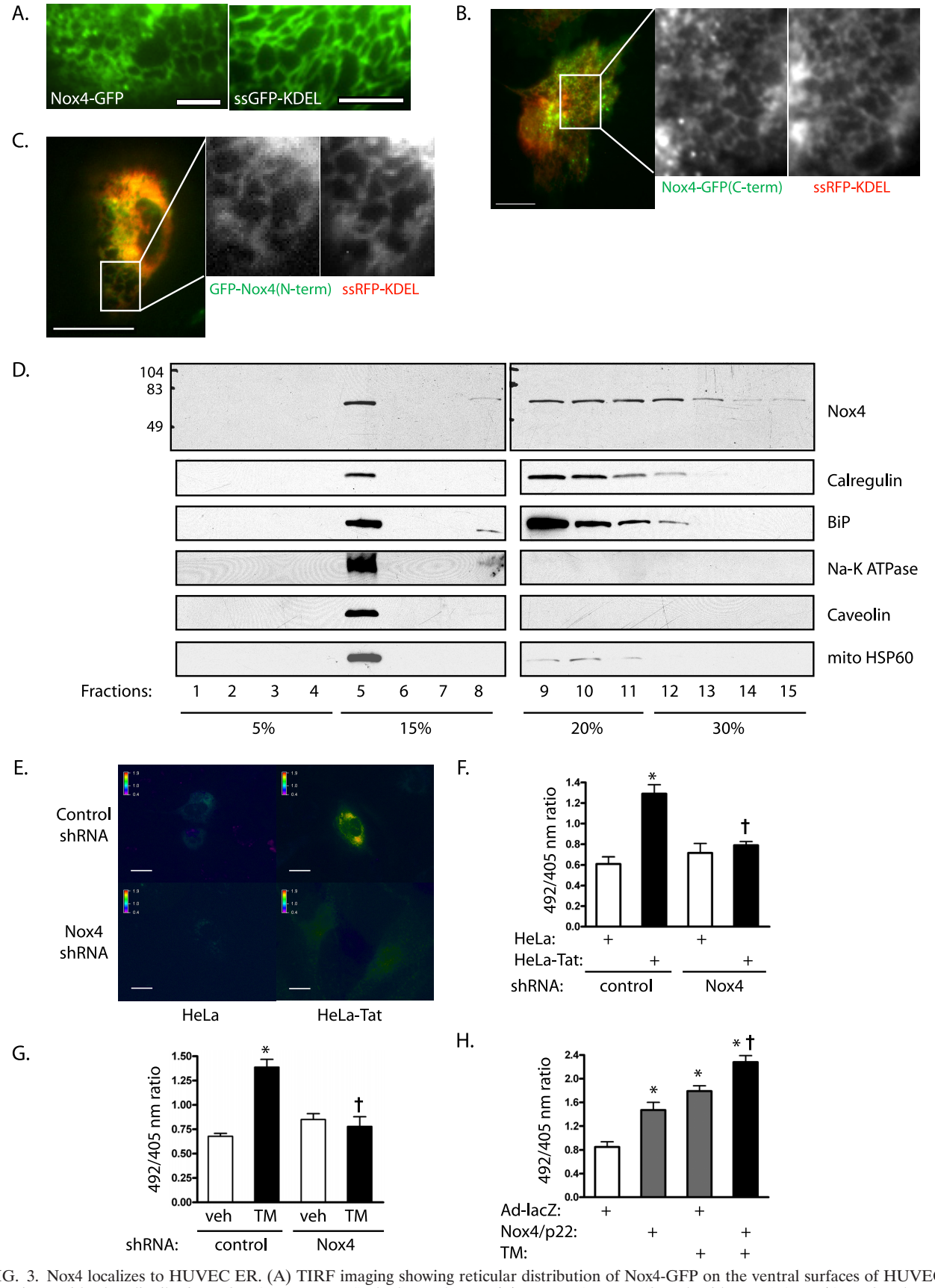

FIG. 3. Nox4 localizes to HUVEC ER. (A) TIRF imaging showing reticular distribution of Nox4-GFP on the ventral surfaces of HUVEC in comparison with the distribution of ssGFP-KDEL. Scale bars, 5 μm. (B) HUVEC cotransfected with Nox4-GFP (GFP fused to the

or DTT (Fig. 4C), and reagent H_2O_2 increased BiP induction (Fig. 4D).

When Tat was used as an agonist, ER-targeted catalase and the oxidase inhibitor diphenylene iodonium prevented BiP induction (Fig. 4E and F), indicating the involvement of ER-localized H_2O_2 in signaling from this agonist. Similar to the response to tunicamycin, Nox4 knockdown completely blocked phosphorylation of JNK and eIF2α and induction of CHOP and BiP by Tat, whereas knockdown of Nox2 had no effect on Tat-induced UPR signaling (Fig. 4G and H). To confirm the involvement of Nox4 in ER stress signaling, Nox4 and $p22^{phox}$ were overexpressed using adenoviral delivery, resulting in eIF2α phosphorylation, induction of CHOP and BiP, and splicing of the XBP-1 transcript (Fig. 4I and J), whereas ER-targeted catalase blocked BiP induction by Nox4 (Fig. 4K). Nox4-dependent H_2O_2 production, therefore, acts upstream of the UPR, mediating ER stress signaling in response to specific agonists, such as tunicamycin and Tat.

Nox4 mediates Ras activation on the ER endomembrane. To gain further support for the role of Nox4 in specific ER signaling events, we examined the involvement of other known signaling pathways, focusing on the agonist Tat. When stimulated acutely with Tat, RhoA and Ras are transiently activated (44). Under these conditions, RhoA acts upstream of Nox4, which in turn leads to downstream Ras activation. Prolonged exposure of HUVEC to Tat-secreting HeLa cells increased RhoA activation, which appeared on day 1 and was sustained through day 7 (Fig. 5A), and antibodies against Tat blocked RhoA activation (Fig. 5B). The Rho binding domain of rhotekin, a RhoA-specific effector, was fused to GFP (RhBD-GFP) to visualize sites of endogenous RhoA-GTP (24). To demonstrate the specificity of this probe, HUVEC were stimulated with the RhoA agonist lysophosphatidic acid, causing translocation of RhBD-GFP to submembranous sites of RhoA activation (Fig. 5C). Whereas HUVEC exposed to control HeLa cells displayed diffuse localization of the reporter, 3 days of exposure to Tat caused marked targeting of RhBD-GFP to the ER, labeled by ssRFP-KDEL (Fig. 5D). To confirm activation of RhoA on the ER surface, ER-specific iodixanol gradient fractions were pooled and examined for RhoA. Significant levels of RhoA were found in ER fractions, unaltered by Tat treatment. However, pulldown of RhoA-GTP from ER fractions indicated activation of RhoA associated with the ER in response to Tat (Fig. 5E). In addition, expression of RhoA(N19) blocked H_2O_2 production by the ER, as assessed by HyPer-ER ratio imaging (Fig. 5F). Thus, RhoA appears to be activated on the ER surface upstream of Nox4.

Notably, Ras activation was also found to be robust and sustained following exposure to Tat-secreting HeLa cells, lasting through day 7 (Fig. 6A), and to be decreased by coincubation with antibodies against Tat (Fig. 6B). Endogenous Ras-GTP was visualized by expression of GFP fused to a triconcatenated Ras binding domain of Raf [RBD3(R59A)-GFP]. The redundant Ras binding domains increased the sensitivity of the probe, while the R59A mutation loosened binding to Ras-GTP to avoid quantitative Ras-GTP sequestration (3). Oligomerized wild-type RBD increased cell attrition over the duration of the experiment, and this probe was not used (data not shown). Exposure of HUVEC to Tat-secreting HeLa cells caused translocation of RBD3(R59A)-GFP to the ER, marked by colocalization with ssRFP-KDEL (Fig. 6C and D). Plasma membrane targeting of the probe was not noted following exposure to Tat. In contrast, short-term stimulation of HUVEC with VEGF caused membrane targeting of RBD3(R59A)-GFP (Fig. 6E), while treatment with the Ras prenylation inhibitor simvastatin blocked Tat-induced translocation of this probe to the ER (Fig. 6F), documenting the specificity of the probe. Further, knockdown of Nox4 resulted in loss of ER-associated Ras-GTP (Fig. 6C and D), as well as loss of global Ras activation (Fig. 6G), suggesting activation of ER-associated Ras downstream of Nox4. ER density gradient fractions confirmed the association of K-Ras with ER endomembranes under basal conditions (Fig. 6H). Similar to the situation with RhoA, exposure to Tat caused activation of K-Ras associated with the ER, as assessed by pulldown (Fig. 6H). Finally, ER-targeted catalase also blocked Tat-induced Ras activation (Fig. 6I). In sum, these data suggest that Tat initiates Nox4-dependent signaling, activating K-Ras locally on the ER surface.

The activation and targeting of both RhoA and Ras to the ER further confirmed the action of Nox4 on the ER, as these GTPases function upstream and downstream of Nox4, respectively. Localization of the RhoA/Nox4/Ras pathway to the ER surface is also consistent with its potential involvement in ER stress signaling. HUVEC express significant levels of K- and N-Ras but very little H-Ras (not shown). Interestingly, Tat-dependent JNK and eIF2α phosphorylation and CHOP and BiP induction were selectively blocked by knockdown of K-Ras, but not N-Ras (Fig. 7A to C), correlating with activation of K-Ras in ER membrane fractions. In addition, expression of

Nox4 C terminus) and ssRFP-KDEL, imaged with TIRF optics. Scale bar, 20 μm. The expansions of the boxed area show green and red channels. (C) HUVEC cotransfected with GFP-Nox4 (GFP fused to the Nox4 N terminus) and ssRFP-KDEL, imaged with TIRF optics. Scale bar, 20 μm. (D) HUVEC lysate fractionated on a 5 to 30% discontinuous iodixanol gradient, immunoblotted for ER (calregulin and BiP), plasma membrane (Na-K ATPase and caveolin), or mitochondrial (HSP60) markers. Fractions 9 to 12 were enriched in ER markers. Fraction 5 contained a nonspecific low-density particulate fraction from multiple membrane sources. (E) HUVEC were infected with lentivirus containing control or Nox4 shRNA and then transfected with HyPer-ER and exposed to HeLa or HeLa-Tat cells for 3 days. Live-cell imaging was performed in the presence of cocultured cells. Representative fields are shown; scale bars, 20 μm. (F) HyPer ratios were compared in the preceding experimental groups. The means and SEM of 6 determinations are shown. *, $P < 0.001$ from control; †, $P < 0.001$ from HeLa-Tat with control shRNA. (G) HyPer ratios were obtained from HUVEC following lentiviral infection with the indicated shRNA and following exposure to vehicle (0.001% DMSO; veh) or tunicamycin (TM; 10 μg/ml) for 16 h. The means and SEM of 7 to 11 determinations are shown. *, $P < 0.001$ from control; †, $P < 0.001$ from TM with control shRNA. (H) HUVEC transfected with HyPer-ER were transduced with control adenovirus (*lacZ*) or Nox4 and $p22^{phox}$ for 3 days and/or treated with tunicamycin for 16 h, as indicated. The means and SEM of 17 to 25 determinations are shown. *, $P < 0.01$ from Ad-lacZ control; †, $P < 0.01$ from TM and Nox4/p22. TM alone was not different from Nox4/p22 ($P > 0.05$).

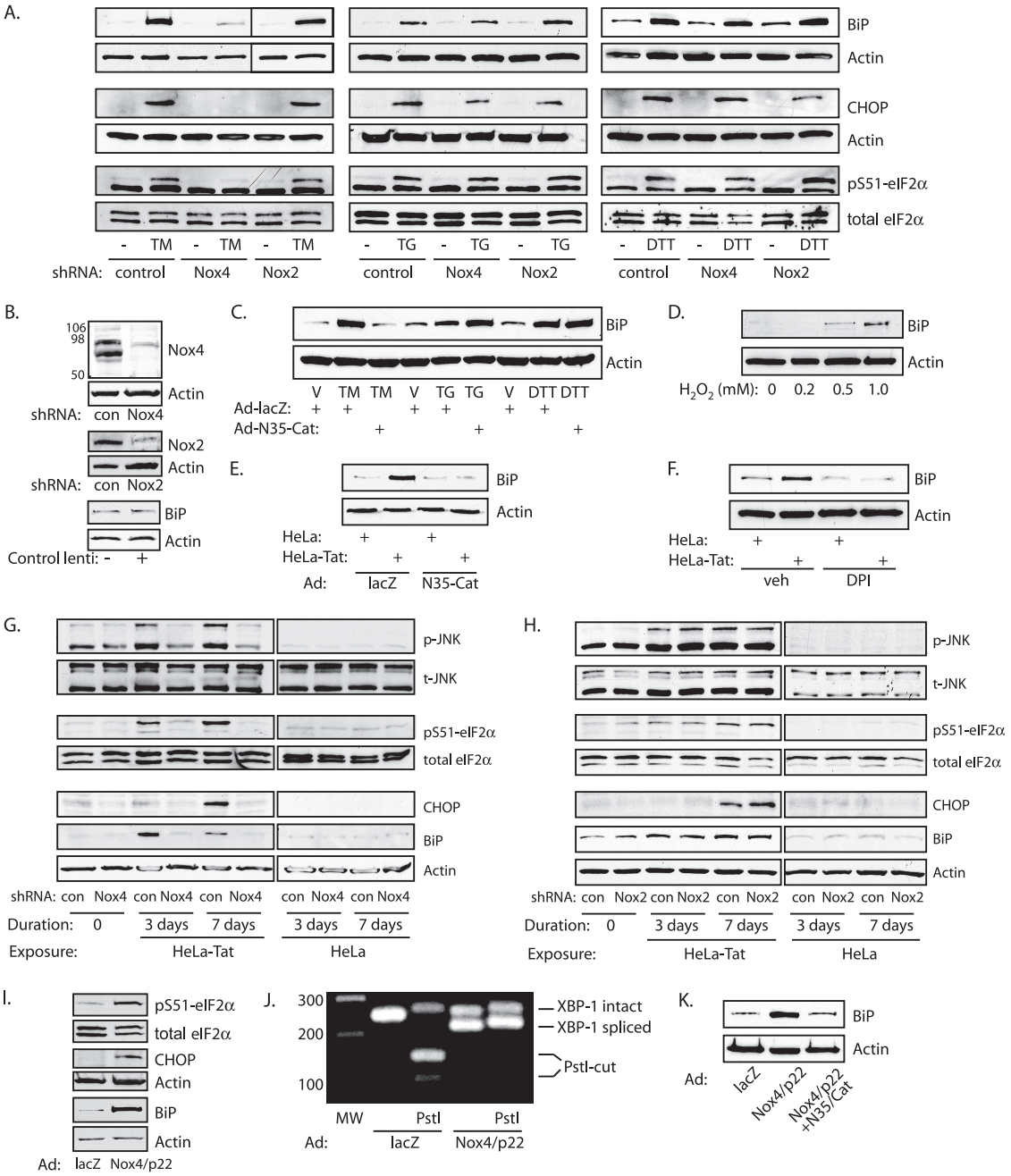

FIG. 4. Nox4 mediates tunicamycin and Tat-induced UPR. (A) Lentiviral knockdown of Nox4 or Nox2 preceded exposure of HUVEC to tunicamycin (TM) (10 μg/ml), thapsigargin (TG) (0.4 μM), or DTT (2 mM) for 16 h. (B) Efficacy of knockdown. con, control; lenti, lentivirus. Numbers at the left indicate molecular mass markers in kilodaltons. (C) HUVEC were transduced with control (lacZ) or N35-Cat adenovirus and then exposed to vehicle (0.001% DMSO) (V), TM, TG, or DTT for 16 h. (D) HUVEC were exposed to the indicated concentrations of H_2O_2 for 16 h, and BiP was assessed by immunoblotting. (E) Cells were transduced with Ad-lacZ or Ad–N35-Cat and cocultured with HeLa or HeLa-Tat cells for 3 days. BiP expression is shown. (F) Cells were cocultured with HeLa or HeLa-Tat cells in the presence of vehicle (0.001% DMSO) or diphenylene iodonium (DPI) (10 μM) for 3 days, and BiP was assessed. (G) Following knockdown of Nox4, untreated HUVEC (lanes 1 and 2) or HUVEC cocultured with HeLa-Tat (lanes 3 to 6) or HeLa (lanes 7 to 10) cells for 3 or 7 days were immunoblotted as indicated. Knockdown of Nox4 completely blocked phosphorylation of JNK and eIF2α and induction of CHOP and BiP by HeLa-Tat cells. UPR markers were uninduced in HeLa-exposed cells. (H) Conditions were similar to those in panel G except following Nox2 instead of Nox4 knockdown. Nox2 knockdown had no effect on activation of the UPR. (I) Overexpression of Nox4 and $p22^{phox}$ by adenoviral transduction increased eIF2α phosphorylation and CHOP and BiP induction compared to Ad-lacZ infection. The blots are representative of 2 to 4 experiments. (J) RT-PCR of XBP-1 transcript demonstrating splicing of XBP-1 3 days after infection with Ad-Nox4/Ad-p22. (K) Nox4 and $p22^{phox}$ were overexpressed in the presence or absence of N35-Cat, as indicated, and the cells were immunoblotted for BiP.

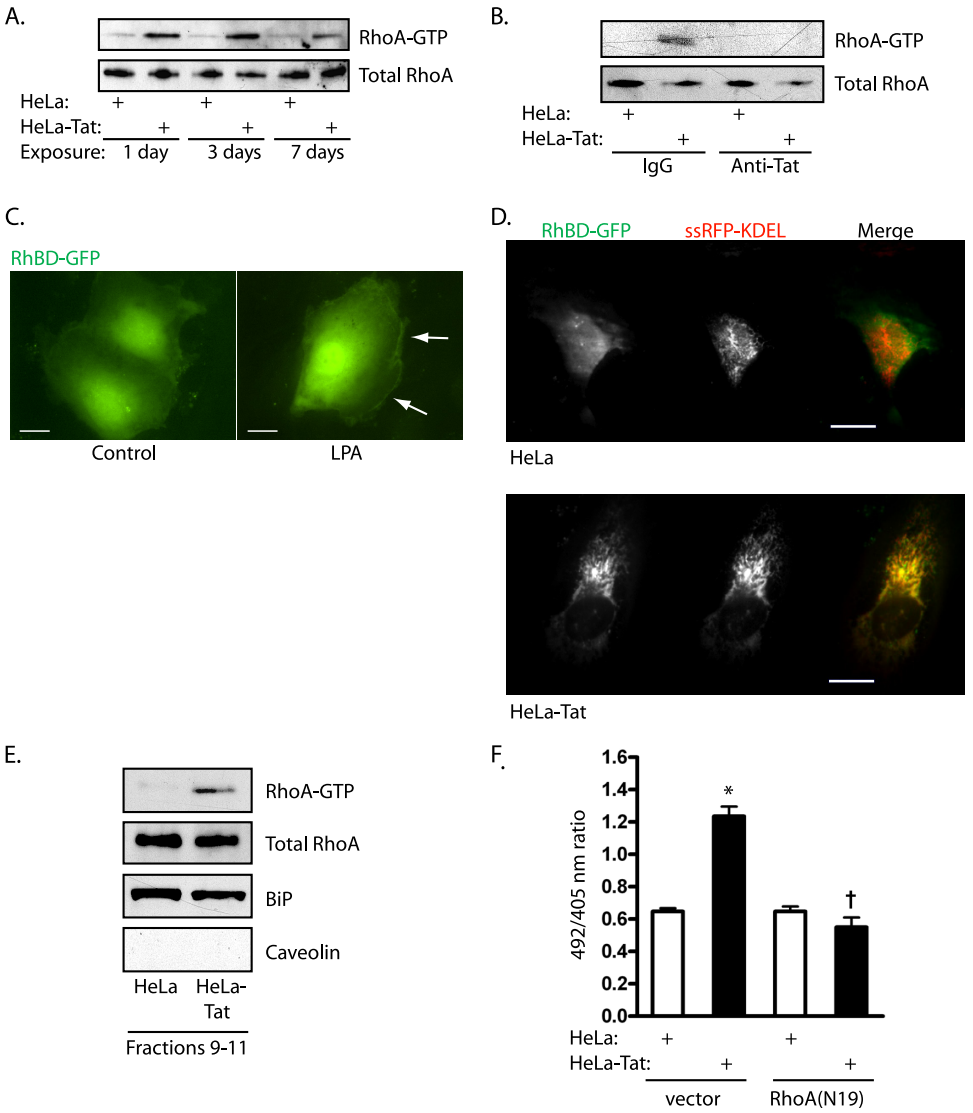

FIG. 5. Tat activates RhoA on the ER. (A) Pulldowns were used to assess activation of RhoA after 1, 3, and 7 days of exposure to HeLa or HeLa-Tat cells. (B) RhoA activity was assessed by pulldown after 1 day of exposure to HeLa or HeLa-Tat cells in the presence of anti-Tat or control antibodies. (C) HUVEC transfected with RhBD-GFP, to visualize sites of endogenous RhoA-GTP, and stimulated with lysophosphatidic acid (LPA) (10 μM). RhBD-GFP translocated to linear cortical structures (arrows). Scale bar, 20 μm. (D) HUVEC were cotransfected with RhBD-GFP and ssRFP-KDEL, the latter to mark the ER. TIRF imaging revealed typical reticular ventral ER, with nonlocalized RhoA activation after 3 days of exposure to HeLa (top) but extensive relocalization of active RhoA to ER after 3 days of exposure to HeLa-Tat cells. Scale bar, 20 μm. (E) HUVEC were cocultured with HeLa or HeLa-Tat cells for 1 day and subjected to iodixanol density gradient fractionation. Fractions 9 to 11 were pooled and split for immunoblots (RhoA, the ER marker BiP, and the plasma membrane marker caveolin) and for pulldown for active RhoA-GTP. (F) HUVEC were cotransfected with HyPer-ER and either empty vector or RhoA(N19) and cocultured with HeLa or HeLa-Tat cells for 3 days, followed by measurement of 492/405 ratios. The means and SEM of 12 to 15 determinations are shown. *, $P < 0.001$ from HeLa control; †, $P < 0.001$ from HeLa-Tat control.

RhoA (N19) also blocked indicators of the UPR (Fig. 7D). Thus, RhoA, Nox4, and Ras appear to signal on the ER surface to mediate the Tat-dependent ER stress response.

We next examined two pathways downstream from the well-known Ras effectors Raf and p85/phosphatidylinositol 3-kinase (PI3K) and found that Tat caused sustained phosphorylation of ERK through day 7 of exposure (Fig. 8A), suppressed by the MEK inhibitor PD098059 (Fig. 8B). In contrast, Tat did not activate the Akt/mTOR/p70S6K pathway downstream from type I PI3K (Fig. 8A). As a control, phosphorylation of these kinases was demonstrated following VEGF stimulation (not shown). The differential activation of Ras effectors is consistent with endomembranous Ras activation. Activation of the PI3K/Akt pathway by Ras restricted to the ER, for instance, remains low compared to Ras directed to the Golgi or plasma membrane (11). ERK phosphorylation occurred downstream from the ER-based Nox4 pathway, as it was completely suppressed by RhoA(N19) expression and Nox4 knockdown, as well as by specific knockdown of K-Ras (Fig. 8C to F).

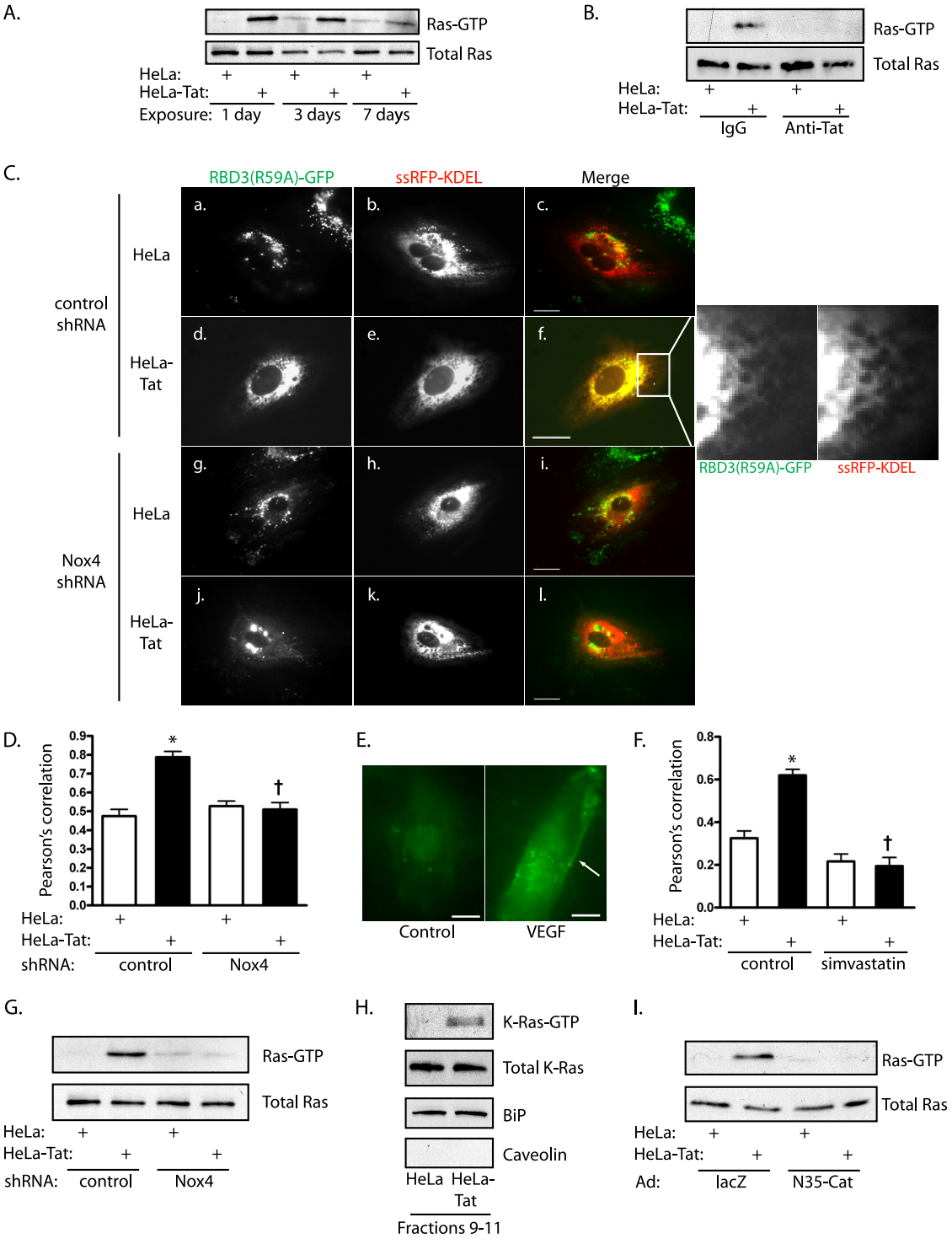

FIG. 6. Tat causes Nox4-dependent Ras activation on the ER. (A) HUVEC were cocultured with HeLa or HeLa-Tat cells for 1 to 7 days, and active Ras was assessed by pulldown. (B) Ras activity was assessed by pulldown after 1 day of exposure to HeLa or HeLa-Tat cells in the presence of anti-Tat or control antibodies. (C) HUVEC were cotransfected with RBD3(R59A)-GFP, to mark sites of endogenous Ras-GTP accumulation and with ssRFP-KDEL to mark the ER. The cells were cocultured with HeLa (a to c and g to i) or HeLa-Tat (d to f and j to l) for 3 days following infection with control (a to f) or Nox4 (g to l) shRNA. Scale bars, 20 μm. The enlargement of the boxed area of image f shows GFP and RFP. (D) Colocalization was quantified for the experimental groups using Pearson's correlation. Shown are means and SEM of 7 determinations. *, $P < 0.01$ from control; †, $P < 0.01$ from HeLa-Tat with control shRNA. (E) HUVEC transfected with RBD3(R59A)-GFP were stimulated with VEGF (50 ng/ml). RBD3(R59A)-GFP was imaged with TIRF optics, demonstrating translocation to the plasma membrane (arrow). Scale bar, 20 μm. (F) HUVEC were cotransfected with RBD3(R59A)-GFP and ssRFP-KDEL and then cocultured with HeLa or HeLa-Tat cells in the presence or absence of simvastatin (10 μM) for 3 days. Colocalization of the probes was quantified using Pearson's correlation. Shown are the means and SEM of 14 to 29 determinations. *, $P < 0.001$ from HeLa control; †, $P < 0.001$ from HeLa-Tat control. (G) Ras-GTP was assessed by pulldown under the indicated conditions after exposure to HeLa or HeLa-Tat cells for 3 days. (H) HUVEC were cocultured with HeLa or HeLa-Tat cells for 1 day and subjected to iodixanol density gradient fractionation. Fractions 9 to 11 were pooled and split for immunoblots (K-Ras, the ER marker BiP, and the plasma membrane marker caveolin) and for pulldown for active K-Ras–GTP. (I) Ras-GTP was assessed by pulldown under the indicated conditions, after exposure to HeLa or HeLa-Tat cells for 3 days.

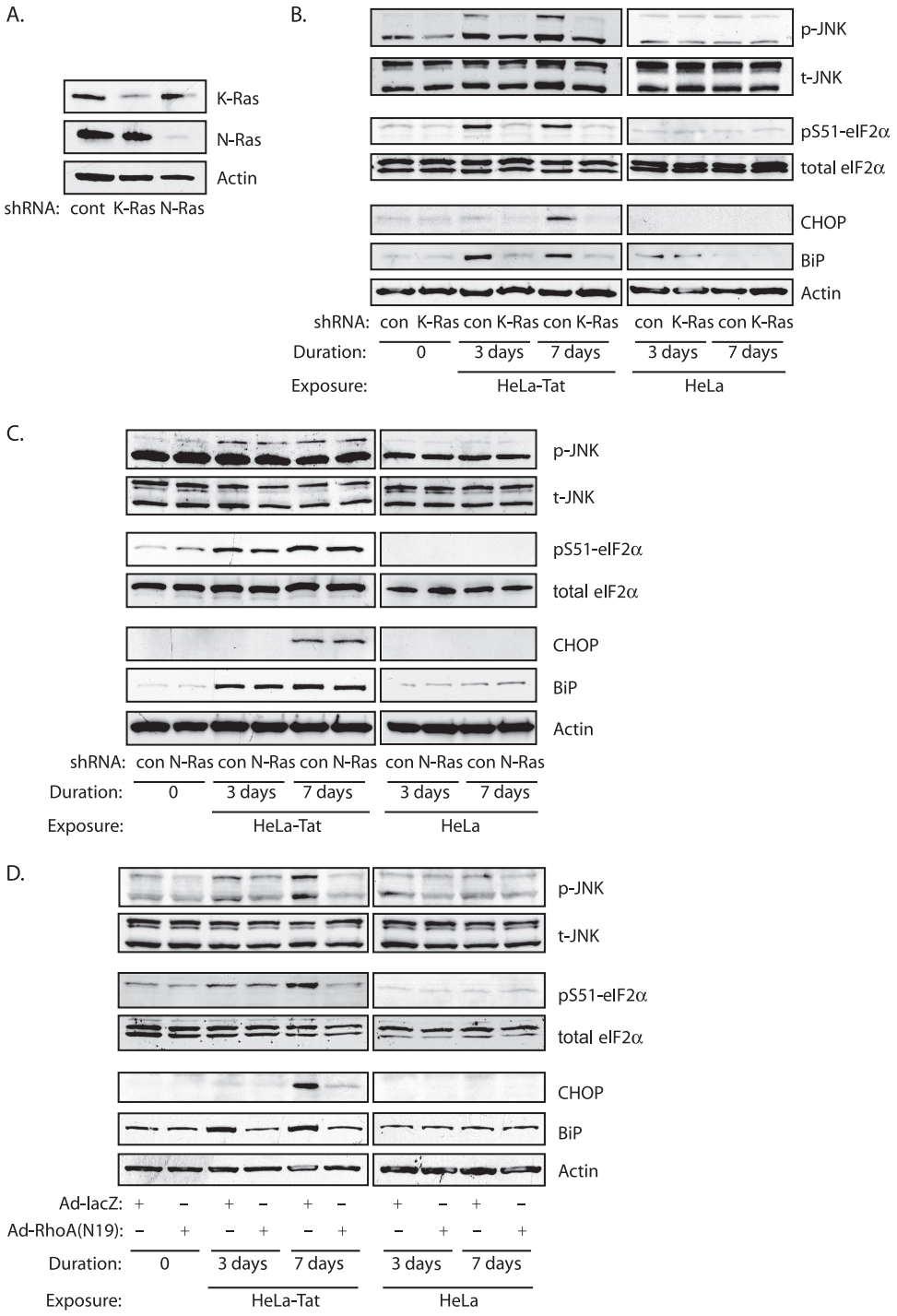

FIG. 7. Tat activates the UPR through K-Ras and RhoA. (A) shRNA specific for either K-Ras or N-Ras was delivered by lentivirus. Immunoblots for K-Ras and N-Ras are shown. (B) UPR was assessed by immunoblotting for phosphorylation of JNK and eIF2α and CHOP and BiP induction under the indicated conditions. K-Ras knockdown completely blocked UPR. (C) The same experimental conditions as for panel B, except following N-Ras knockdown. (D) UPR was assessed as for panel B, except in the presence or absence of dominant-negative RhoA(N19).

Nox4/Ras signaling induces autophagy, which increases cell survival and differentiation. Recent studies have demonstrated that ER stress often triggers autophagy, which is an additional, highly conserved degradation pathway linked to ERK activation (6, 30, 32, 47). Not surprisingly, a number of proteins that control autophagy reside on the ER, and autophagic membranes are thought to be derived from ER lipids (4, 33). Within 3 days of exposure to Tat, several markers of autophagy increased. First, LC3/Atg8 was converted to a higher-mobility form (LC3-II), indicative of conjugation to phosphati-

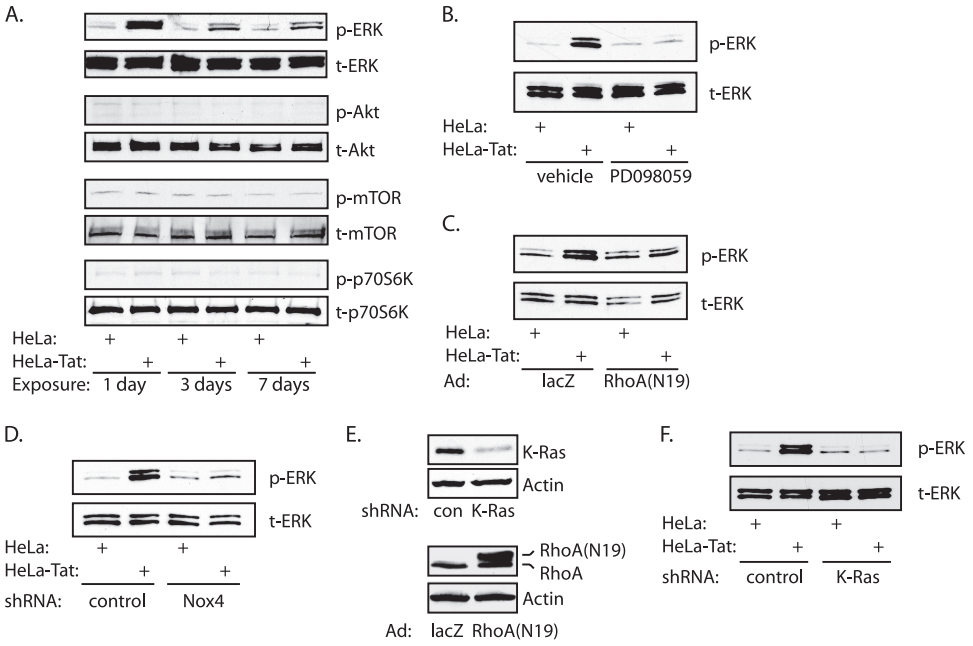

FIG. 8. ERK, but not Akt, is activated by Tat downstream of K-Ras. (A) HUVEC were cocultured with HeLa or HeLa-Tat cells as indicated. ERK phosphorylation persisted for 7 days, whereas no detectable phosphorylation of Akt, mTOR, or p70S6K was noted. (B) Phospho-ERK was assessed in HUVEC cocultured with HeLa or HeLa-Tat cells for 1 day in the presence of vehicle (0.001% DMSO) or PD098059 (20 mM). (C and D) HUVEC were cocultured with HeLa or HeLa-Tat cells for 3 days following RhoA(N19) expression or Nox4 knockdown. (E) Immunoblot demonstrating the efficacy of shRNA against K-Ras (top) and expression of dominant-negative RhoA(N19). The form of RhoA(N19)with slower mobility is from Myc tag. (F) K-Ras knockdown blocked ERK phosphorylation.

dylethanolamine and formation of early autophagosomes (Fig. 9A). Second, LC3-GFP, normally distributed diffusely in the cytosol, formed dots, characteristic of autophagosome formation (Fig. 9B and C). Lipidated LC3 is incorporated into autophagosomal membranes; thus, LC3-GFP could clearly be seen outlining vesicular structures (Fig. 9B, boxed area). Third, transmission electron microscopy sections confirmed the formation of numerous autophagosomes, some containing densely packed membrane stacks characteristic of reticulophagy (Fig. 9D) (6). Dilated ER lumens were also noted, consistent with ER stress. Autophagy induced in association with ER stress was Nox4 dependent, as knockdown of Nox4 suppressed Tat-induced LC3-II formation, overexpression of Nox4 increased LC3-II formation, and ER-targeted catalase blocked Nox4-dependent LC3-II formation (Fig. 9E to G). In addition, LC3-II formation was blocked by K-Ras knockdown and MEK1 inhibition (PD095089) (Fig. 9H and I), consistent with activation of autophagy downstream from an ER-based Nox4/K-Ras/ERK pathway.

Initiation of autophagy has been shown to exert protective effects in yeast and mammalian cells against the cell death response to ER stress (6, 30). Tat-induced autophagy was inhibited by the class III PI3K inhibitor 3-methyl adenine (Fig. 10A), which by itself increased cell death in control cells by a modest amount (Fig. 10B). Upon exposure of cells to Tat for 5 days, untreated cells showed no increase in cell death, whereas 3-methyl adenine-treated cells had marked increases in cell death, in combination with Tat (Fig. 10B). To substantiate these results, autophagy was also suppressed by knockdown of the autophagic protein Atg5 (Fig. 10C), which again allowed cell death to occur following exposure to Tat (Fig. 10D). Finally, exposure of HUVEC to Tat for 3 days accelerated tube formation in 3-dimensional Matrigel, indicating endothelial differentiation (Fig. 10E and F). Suppression of autophagy with 3-methyl adenine, however, caused complete failure of cells to attain a reticular, branching morphology, with cells instead forming irregular spheroid clusters (Fig. 10E). Thus, autophagy not only protects against cell death following ER stress, but permits morphological differentiation of endothelial cells.

DISCUSSION

The integrity of a cell's nascent proteins reflects the homeostatic balance of a number of cellular conditions, including global and ER redox status, amino acid and energy sufficiency, and synthetic demands. Consequently, a variety of stress pathways arise from the ER in response to poorly folded proteins. In this capacity, reactive oxidants generated as a consequence of ER stress are thought to represent late effectors of the UPR leading to oxidative stress and cell death. Much less evidence supports an additional homeostatic signaling role for oxidants upstream of the UPR. In a recent study, the antioxidant butylated hydroxyanisole (BHA) was found to decrease the UPR response to misfolded FVIII, allowing the possibility of an upstream role for oxidants (25). In that study, however, BHA improved rather than worsened protein folding and secretion, and oxidant production was CHOP dependent, suggesting that oxidants were produced as a downstream consequence of the

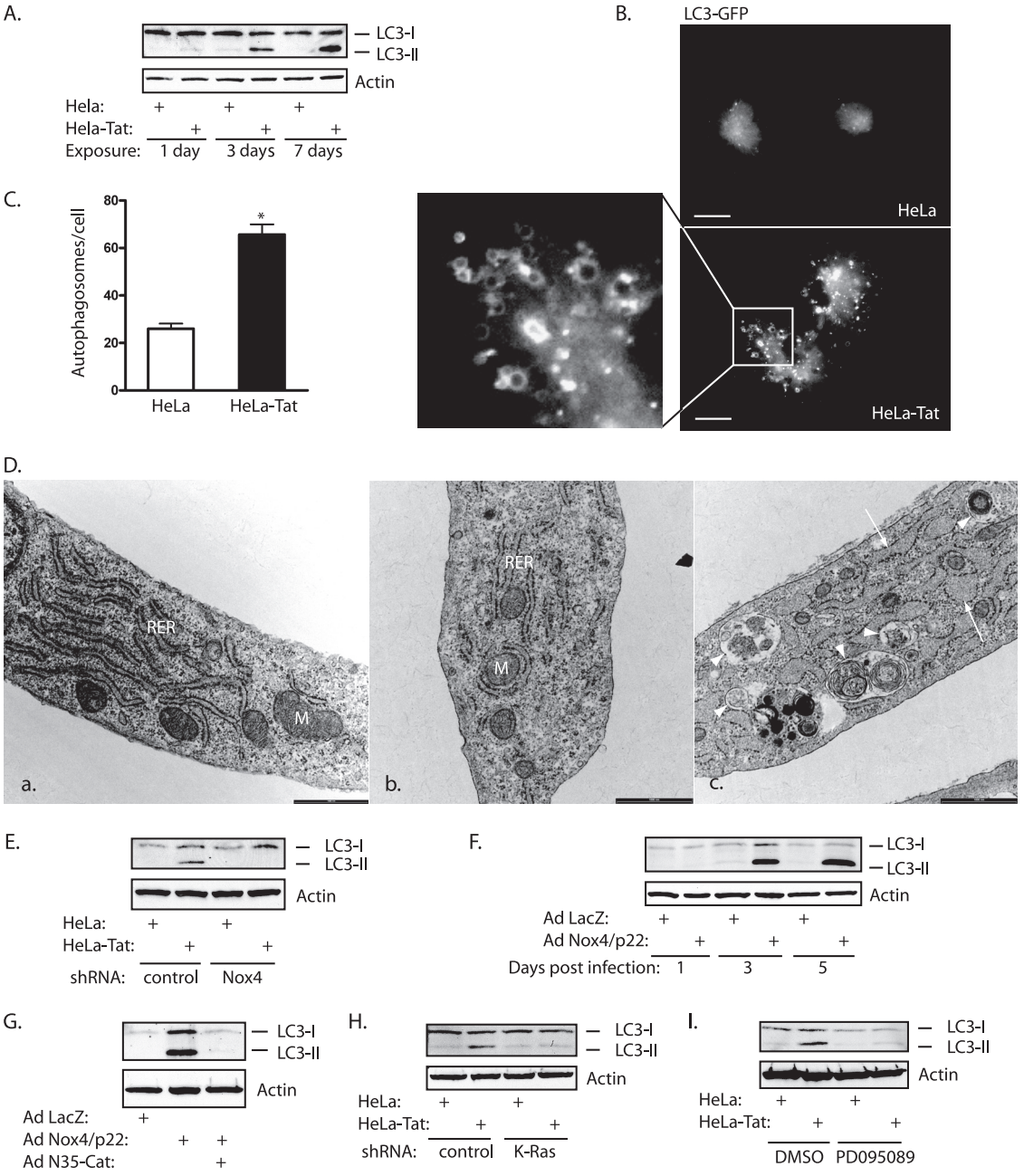

FIG. 9. Nox4 mediates autophagy. (A) Immunoblot for LC3 showing formation of a lipidated, higher-mobility form (LC3-II) with 3 and 7 days of exposure to HeLa-Tat cells. (B) HUVEC were transfected with LC3-GFP and cocultured with HeLa or HeLa-Tat cells for 3 days. The formation of numerous LC3-GFP-positive dots was seen with HeLa-Tat exposure. The enlargement of the boxed area shows the vesicular nature of larger LC3-GFP-positive structures, consistent with autophagosome formation. Scale bar, 20 μm. (C) Quantification of LC3-GFP dots per cell. *, $P < 0.001$. The error bars indicate SEM. (D) Scanning electron microscopy of normal, unstimulated HUVEC (a) or HUVEC exposed to HeLa cells (b) or HeLa-Tat cells (c) for 5 days. M, mitochondrion; RER, rough ER. The normal morphology of RER is seen in images a and b. Following exposure to HeLa-Tat cells, the ER becomes swollen, with dilated lumens (image c, arrows), with numerous autophagosomes (arrowheads) with variable contents. These include tightly packed lamellar membranes suggesting ER ingestion. Scale bar, 1,000 nm. (E to I) HUVEC were immunoblotted for endogenous LC3 after exposure to HeLa or HeLa-Tat cells. (E and F) Nox4 knockdown reduced LC3-II formation from Tat, whereas expression of Nox4 and $p22^{phox}$ greatly increased LC3-II formation. (G) N35-Cat blocked LC3-II formation. Suppression of Ras/ERK signaling through K-Ras knockdown (H) or MEK inhibition (I) (20 mM PD095089 versus vehicle) also reduced LC3-II formation after 3 days of exposure to HeLa-Tat cells.

UPR and subsequently worsened protein folding in a positive-feedback cycle.

In the present study, we found clear evidence that Nox4 initiates oxidative signaling on the ER upstream of the UPR. We first documented H_2O_2 production by the ER. Although prior studies have used nonspecific probes, such as dichlorofluorescein or dihydroethidium, to detect global cellular oxidant production, the specific production of H_2O_2 *in situ* by the

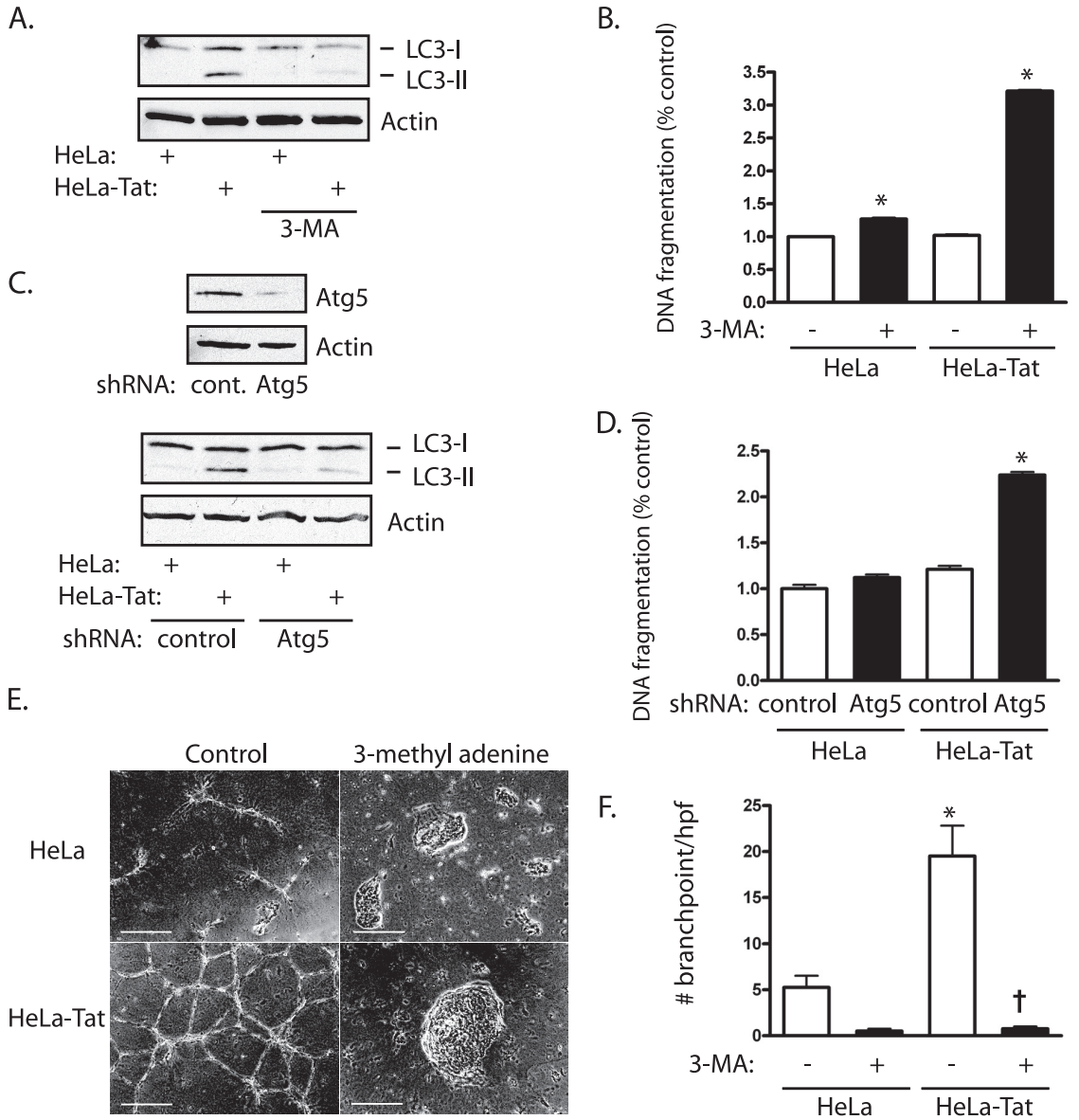

FIG. 10. Autophagy protects Tat-exposed cells. (A) 3-Methyl adenine (3-MA) (5 mM) reduced LC3-II formation after 3 days of exposure to HeLa-Tat cells, indicating inhibition of autophagy. (B) HUVEC were exposed to HeLa or HeLa-Tat cells for 5 days, with addition of 3-MA for the final 2 days. The means and SEM of 4 determinations are shown. *, $P < 0.001$ from the respective control without 3-MA. (C) Knockdown of Atg5 by shRNA (top) decreased LC3-II formation after 3 days of exposure to HeLa-Tat cells. (D) Atg5 knockdown increased cell death in HeLa-Tat-exposed HUVEC; *, $P < 0.001$ from control. The means and SEM of 4 determinations are shown. (E) Phase-contrast of HUVEC plated in thick Matrigel slabs and exposed to HeLa or HeLa-Tat cells for 3 days. The addition of 3-MA (5 mM) caused the cells to form 3-dimensional spheroid clusters without typical branching tube structures. Scale bars, 500 μm. (F) Branch points were counted to quantify differentiation into tube structures. The means and SEM of 8 determinations are shown. *, $P < 0.001$ from control; †, $P < 0.001$ from HeLa-Tat without 3-MA.

ER of live cells has not previously been reported. Interestingly, we found the HyPer ratio of the ER under basal conditions to be similar to that of HyPer free in the cytosol, suggesting relatively low H_2O_2 concentrations in the unstressed ER despite its relatively oxidized redox potential. Conversely, we found that the stressed ER may increase its H_2O_2 levels; however, the production of H_2O_2 by the ER itself does not appear to be a universal feature of ER stress. Tunicamycin and Tat caused measurable increases in ER H_2O_2 levels, whereas thapsigargin and DTT decreased ER H_2O_2, even at time points following the induction of CHOP. These findings suggest that the oxidative stress that occurs downstream of the UPR and is associated with cell death may arise substantially from non-ER sources. Suppression of mitochondrial respiration, for instance, blocks ROS generation and cell death in ER-stressed yeast and mammalian cells, although it may be difficult to distinguish the effects of ROS suppression from those of loss of other mitochondrial functions (15, 16).

Further support for a specific signaling function of ER H_2O_2 was obtained by linkage of such oxidants with Nox4. Notably, ER H_2O_2 production from tunicamycin and Tat was eliminated by knockdown of Nox4, which also blocked the UPR

responses by these agonists, but not by thapsigargin or DTT. Thus, Nox4-derived ER H_2O_2 appears to function as an agonist-specified signal capable of initiating the UPR. Like other Nox members, Nox4 may function primarily as a signaling enzyme, with specific rather than global stress or metabolic effects. Nox4 therefore differs from Ero-1, which is thought to produce H_2O_2 as a constitutive by-product during the O_2-dependent oxidation of PDI and also late in uncompensated ER stress leading to cell death (13, 26). While our data suggest that Nox4 itself is the principal source of ER H_2O_2 under certain conditions, it is also possible that Nox4 causes an increase in oxidant production secondarily through Ero-1, a possibility we have not excluded. Attempts to implicate Ero-1 as a source of oxidants in mammalian cells have not been successful, in part because of the dual isoforms present (15, 26). Notably, organisms such as *Caenorhabditis elegans* and *Saccharomyces cerevisiae* that have only one *ero-1* gene do not possess a Nox4 ortholog.

The relevance of Nox4-dependent ER signaling to cell fate was further studied using HIV-1 Tat. Tat is found circulating in the blood of HIV-infected patients and is thought to contribute to AIDS-related vasculopathy and encephalopathy and thus represents a physiologically relevant ER stressor (2, 29, 39, 46). We found that in response to Tat, Nox4-dependent H_2O_2 production was linked to Ras activation spatially, on the ER surface, and functionally, upstream of the UPR. Such cooperation between the Ras and Nox proteins has been suggested to occur at the plasma membrane during mitogenic signaling from lactosylceramide and angiotensin II (1, 8), although it has not been previously reported on interior membranes. However, Ras is known to be activated on the ER surface in response to mitogens or PKC activation (9, 11). Thus, restriction of a Nox4-Ras pathway to the ER surface is consistent with the importance of subcellular localization to signal fidelity for both the Ras and Nox proteins (31, 38). While oxidative modification of Ras is known to directly activate Ras (22), the mechanism of Ras activation by Nox4 remains unknown. Also unclear at this point is the mechanism by which Tat causes ER stress. Tat is known to engage a number of surface receptors, such as chemokine, integrin, and growth factor receptors, and can also translocate into the cell to interact with transcriptional regulators, such as p300/CBP. Thus, certain parts of proliferative or gene expression pathways may be directly or indirectly activated out of physiologic context, perhaps leading to ER stress.

Further evidence for the importance of a local Nox4/Ras pathway in ER signaling was obtained by examining its effect on the induction of autophagy, which is another process triggered by events occurring on the ER surface. Beclin 1, an essential subunit of the class III PI3K complex that participates in autophagosome formation, resides on the ER, where it is sequestered by Bcl-2 (33). In addition, autophagosomes appear to form from punctate structures that recruit initiator complexes and incorporate Phosphatidylinositol 3-phosphate-enriched lipids from the ER (4). Accordingly, ER stress and the UPR trigger autophagy, leading to degradation and recycling of protein aggregates and parts of the expanded ER (6, 21, 30, 47). Importantly, we found that Nox4-dependent autophagy promotes survival, consistent with the survival function of autophagy in the context of either ER stress or direct activation of the UPR (6, 30). Of note, Nox2 has recently been demonstrated to participate in recruitment of LC3 to phagosomes during microbial killing by phagocytes (20). While we did not find a role for Nox2 in ER stress-initiated autophagy, these findings suggest that different Nox forms may contribute to autophagy triggered by different subcellular structures.

Prior studies have demonstrated that ERK promotes autophagy whereas type I PI3K suppresses it through activation of the powerful autophagy inhibitor mTOR (32, 37). Thus, two principal Ras effectors, Raf and type I PI3K, act divergently with respect to induction of autophagy (32). Accordingly, while untargeted RasV12 has been shown to suppress autophagy through type I PI3K/Akt/mTOR activation (7), our data suggest that asymmetric activation of Ras effectors by Tat, favoring the ERK but not the mTOR pathway, allows a protective autophagic response to be initiated. The basis for such pathway specificity is not known, although it may result in part from restriction of Ras signaling to the ER. Ras directed to different membrane compartments is known to differentially activate various effectors (11), although differential activation of ERK and Akt by ER Ras had not been clearly demonstrated prior to the present study.

In summary, we found evidence that Nox4 contributes significantly to ER-localized H_2O_2 production, which in turn functions as a homeostatic signal to initiate the UPR and autophagy. Cooperation of Nox4 and Ras on an ER platform facilitates these events, which, following Tat-dependent ER stress, prevent cell death and promote differentiation.

ACKNOWLEDGMENTS

We acknowledge the excellent technical skills of Chengxu Liao.

This work was supported by the NHLBI, grants R01-HL061897 and R01-HL067256, and by institutional support for the Molecular and Cellular Imaging Facility from the University of Texas Southwestern.

REFERENCES

1. **Adachi, T., D. R. Pimentel, T. Heibeck, X. Hou, Y. J. Lee, B. Jiang, Y. Ido, and R. A. Cohen.** 2004. S-glutathiolation of Ras mediates redox-sensitive signaling by angiotensin II in vascular smooth muscle cells. J. Biol. Chem. **279:**29857–29862.
2. **Albini, A., G. Barillari, R. Benelli, R. C. Gallo, and B. Ensoli.** 1995. Angiogenic properties of human immunodeficiency virus type 1 Tat protein. Proc. Natl. Acad. Sci. U. S. A. **92:**4838–4842.
3. **Augsten, M., R. Pusch, C. Biskup, K. Rennert, U. Wittig, K. Beyer, A. Blume, R. Wetzker, K. Friedrich, and I. Rubio.** 2006. Live-cell imaging of endogenous Ras-GTP illustrates predominant Ras activation at the plasma membrane. EMBO Rep. **7:**46–51.
4. **Axe, E. L., S. A. Walker, M. Manifava, P. Chandra, H. L. Roderick, A. Habermann, G. Griffiths, and N. T. Ktistakis.** 2008. Autophagosome formation from membrane compartments enriched in phosphatidylinositol 3-phosphate and dynamically connected to the endoplasmic reticulum. J. Cell Biol. **182:**685–701.
5. **Belousov, V. V., A. F. Fradkov, K. A. Lukyanov, D. B. Staroverov, K. S. Shakhbazov, A. V. Terskikh, and S. Lukyanov.** 2006. Genetically encoded fluorescent indicator for intracellular hydrogen peroxide. Nat. Methods **3:**281–286.
6. **Bernales, S., K. L. McDonald, and P. Walter.** 2006. Autophagy counterbalances endoplasmic reticulum expansion during the unfolded protein response. PLoS Biol. **4:**e423.
7. **Berry, D. L., and E. H. Baehrecke.** 2007. Growth arrest and autophagy are required for salivary gland cell degradation in Drosophila. Cell **131:**1137–1148.
8. **Bhunia, A. K., H. Han, A. Snowden, and S. Chatterjee.** 1997. Redox-regulated signaling by lactosylceramide in the proliferation of human aortic smooth muscle cells. J. Biol. Chem. **272:**15642–15649.
9. **Bivona, T. G., S. E. Quatela, B. O. Bodemann, I. M. Ahearn, M. J. Soskis, A. Mor, J. Miura, H. H. Wiener, L. Wright, S. G. Saba, D. Yim, A. Fein, I. Perez de Castro, C. Li, C. B. Thompson, A. D. Cox, and M. R. Philips.** 2006. PKC regulates a farnesyl-electrostatic switch on K-Ras that promotes its association with Bcl-XL on mitochondria and induces apoptosis. Mol. Cell **21:**481–493.

10. **Chen, K., M. T. Kirber, H. Xiao, Y. Yang, and J. F. Keaney, Jr.** 2008. Regulation of ROS signal transduction by NADPH oxidase 4 localization. J. Cell Biol. **181**:1129–1139.
11. **Chiu, V. K., T. Bivona, A. Hach, J. B. Sajous, J. Silletti, H. Wiener, R. L. Johnson II, A. D. Cox, and M. R. Philips.** 2002. Ras signalling on the endoplasmic reticulum and the Golgi. Nat. Cell Biol. **4:**343–350.
12. **Flores, S. C., J. C. Marecki, K. P. Harper, S. K. Bose, S. K. Nelson, and J. M. McCord.** 1993. Tat protein of human immunodeficiency virus type 1 represses expression of manganese superoxide dismutase in HeLa cells. Proc. Natl. Acad. Sci. U. S. A. **90:**7632–7636.
13. **Gross, E., C. S. Sevier, N. Heldman, E. Vitu, M. Bentzur, C. A. Kaiser, C. Thorpe, and D. Fass.** 2006. Generating disulfides enzymatically: reaction products and electron acceptors of the endoplasmic reticulum thiol oxidase Ero1p. Proc. Natl. Acad. Sci. U. S. A. **103:**299–304.
14. **Gu, Y., R. F. Wu, Y. C. Xu, S. C. Flores, and L. S. Terada.** 2001. HIV Tat activates c-Jun amino-terminal kinase through an oxidant-dependent mechanism. Virology **286:**62–71.
15. **Harding, H. P., Y. Zhang, H. Zeng, I. Novoa, P. D. Lu, M. Calfon, N. Sadri, C. Yun, B. Popko, R. Paules, D. F. Stojdl, J. C. Bell, T. Hettmann, J. M. Leiden, and D. Ron.** 2003. An integrated stress response regulates amino acid metabolism and resistance to oxidative stress. Mol. Cell **11:**619–633.
16. **Haynes, C. M., E. A. Titus, and A. A. Cooper.** 2004. Degradation of misfolded proteins prevents ER-derived oxidative stress and cell death. Mol. Cell **15:**767–776.
17. **Heath-Engel, H. M., N. C. Chang, and G. C. Shore.** 2008. The endoplasmic reticulum in apoptosis and autophagy: role of the BCL-2 protein family. Oncogene **27:**6419–6433.
18. **Hitomi, J., T. Katayama, Y. Eguchi, T. Kudo, M. Taniguchi, Y. Koyama, T. Manabe, S. Yamagishi, Y. Bando, K. Imaizumi, Y. Tsujimoto, and M. Tohyama.** 2004. Involvement of caspase-4 in endoplasmic reticulum stress-induced apoptosis and Abeta-induced cell death. J. Cell Biol. **165:**347–356.
19. **Høyer-Hansen, M., L. Bastholm, P. Szyniarowski, M. Campanella, G. Szabadkai, T. Farkas, K. Bianchi, N. Fehrenbacher, F. Elling, R. Rizzuto, I. S. Mathiasen, and M. Jaattela.** 2007. Control of macroautophagy by calcium, calmodulin-dependent kinase kinase-beta, and Bcl-2. Mol. Cell **25:**193–205.
20. **Huang, J., V. Canadien, G. Y. Lam, B. E. Steinberg, M. C. Dinauer, M. A. Magalhaes, M. Glogauer, S. Grinstein, and J. H. Brumell.** 2009. Activation of antibacterial autophagy by NADPH oxidases. Proc. Natl. Acad. Sci. U. S. A. **106:**6226–6231.
21. **Kouroku, Y., E. Fujita, I. Tanida, T. Ueno, A. Isoai, H. Kumagai, S. Ogawa, R. J. Kaufman, E. Kominami, and T. Momoi.** 2007. ER stress (PERK/eIF2alpha phosphorylation) mediates the polyglutamine-induced LC3 conversion, an essential step for autophagy formation. Cell Death Differ. **14:**230–239.
22. **Lander, H. M., J. S. Ogiste, K. K. Teng, and A. Novogrodsky.** 1995. p21ras as a common signaling target of reactive free radicals and cellular redox stress. J. Biol. Chem. **270:**21195–21198.
23. **Lindl, K. A., C. Akay, Y. Wang, M. G. White, and K. L. Jordan-Sciutto.** 2007. Expression of the endoplasmic reticulum stress response marker, BiP, in the central nervous system of HIV-positive individuals. Neuropathol. Appl. Neurobiol. **33:**658–669.
24. **Ma, Z., D. P. Myers, R. F. Wu, F. E. Nwariaku, and L. S. Terada.** 2007. p66Shc mediates anoikis through RhoA. J. Cell Biol. **179:**23–31.
25. **Malhotra, J. D., H. Miao, K. Zhang, A. Wolfson, S. Pennathur, S. W. Pipe, and R. J. Kaufman.** 2008. Antioxidants reduce endoplasmic reticulum stress and improve protein secretion. Proc. Natl. Acad. Sci. U. S. A. **105:**18525–18530.
26. **Marciniak, S. J., C. Y. Yun, S. Oyadomari, I. Novoa, Y. Zhang, R. Jungreis, K. Nagata, H. P. Harding, and D. Ron.** 2004. CHOP induces death by promoting protein synthesis and oxidation in the stressed endoplasmic reticulum. Genes Dev. **18:**3066–3077.
27. **Martyn, K. D., L. M. Frederick, K. von Loehneysen, M. C. Dinauer, and U. G. Knaus.** 2006. Functional analysis of Nox4 reveals unique characteristics compared to other NADPH oxidases. Cell Signal. **18:**69–82.
28. **Merksamer, P. I., A. Trusina, and F. R. Papa.** 2008. Real-time redox measurements during endoplasmic reticulum stress reveal interlinked protein folding functions. Cell **135:**933–947.
29. **Norman, J. P., S. W. Perry, H. M. Reynolds, M. Kiebala, K. L. De Mesy Bentley, M. Trejo, D. J. Volsky, S. B. Maggirwar, S. Dewhurst, E. Masliah, and H. A. Gelbard.** 2008. HIV-1 Tat activates neuronal ryanodine receptors with rapid induction of the unfolded protein response and mitochondrial hyperpolarization. PLoS One **3:**e3731.
30. **Ogata, M., S. Hino, A. Saito, K. Morikawa, S. Kondo, S. Kanemoto, T. Murakami, M. Taniguchi, I. Tanii, K. Yoshinaga, S. Shiosaka, J. A. Hammarback, F. Urano, and K. Imaizumi.** 2006. Autophagy is activated for cell survival after endoplasmic reticulum stress. Mol. Cell. Biol. **26:**9220–9231.
31. **Onken, B., H. Wiener, M. R. Philips, and E. C. Chang.** 2006. Compartmentalized signaling of Ras in fission yeast. Proc. Natl. Acad. Sci. U. S. A. **103:**9045–9050.
32. **Pattingre, S., C. Bauvy, and P. Codogno.** 2003. Amino acids interfere with the ERK1/2-dependent control of macroautophagy by controlling the activation of Raf-1 in human colon cancer HT-29 cells. J. Biol. Chem. **278:**16667–16674.
33. **Pattingre, S., A. Tassa, X. Qu, R. Garuti, X. H. Liang, N. Mizushima, M. Packer, M. D. Schneider, and B. Levine.** 2005. Bcl-2 antiapoptotic proteins inhibit Beclin 1-dependent autophagy. Cell **122:**927–939.
34. **Pedruzzi, E., C. Guichard, V. Ollivier, F. Driss, M. Fay, C. Prunet, J. C. Marie, C. Pouzet, M. Samadi, C. Elbim, Y. O'Dowd, M. Bens, A. Vandewalle, M. A. Gougerot-Pocidalo, G. Lizard, and E. Ogier-Denis.** 2004. NAD(P)H oxidase Nox-4 mediates 7-ketocholesterol-induced endoplasmic reticulum stress and apoptosis in human aortic smooth muscle cells. Mol. Cell. Biol. **24:**10703–10717.
35. **Puhka, M., H. Vihinen, M. Joensuu, and E. Jokitalo.** 2007. Endoplasmic reticulum remains continuous and undergoes sheet-to-tubule transformation during cell division in mammalian cells. J. Cell Biol. **179:**895–909.
36. **Ron, D., and P. Walter.** 2007. Signal integration in the endoplasmic reticulum unfolded protein response. Nat. Rev. Mol. Cell Biol. **8:**519–529.
37. **Scott, R. C., O. Schuldiner, and T. P. Neufeld.** 2004. Role and regulation of starvation-induced autophagy in the Drosophila fat body. Dev. Cell **7:**167–178.
38. **Terada, L. S.** 2006. Specificity in reactive oxidant signaling: think globally, act locally. J. Cell Biol. **174:**615–623.
39. **Terada, L. S., Y. Gu, and S. C. Flores.** 2000. AIDS vasculopathy. Am. J. Med. Sci. **320:**379–387.
40. **Van Buul, J. D., M. Fernandez-Borja, E. C. Anthony, and P. L. Hordijk.** 2005. Expression and localization of NOX2 and NOX4 in primary human endothelial cells. Antioxid. Redox Signal **7:**308–317.
41. **Vergés, E., N. Colomina, E. Gari, C. Gallego, and M. Aldea.** 2007. Cyclin Cln3 is retained at the ER and released by the J chaperone Ydj1 in late G1 to trigger cell cycle entry. Mol. Cell **26:**649–662.
42. **Wilson, S. J., E. H. Tsao, B. L. Webb, H. Ye, L. Dalton-Griffin, C. Tsantoulas, C. V. Gale, M. Q. Du, A. Whitehouse, and P. Kellam.** 2007. X box binding protein XBP-1s transactivates the Kaposi's sarcoma-associated herpesvirus (KSHV) ORF50 promoter, linking plasma cell differentiation to KSHV reactivation from latency. J. Virol. **81:**13578–13586.
43. **Wu, R. F., Y. Gu, Y. C. Xu, S. Mitola, F. Bussolino, and L. S. Terada.** 2004. Human immunodeficiency virus type 1 Tat regulates endothelial cell actin cytoskeletal dynamics through PAK1 activation and oxidant production. J. Virol. **78:**779–789.
44. **Wu, R. F., Z. Ma, D. P. Myers, and L. S. Terada.** 2007. HIV-1 Tat activates dual Nox pathways leading to independent activation of ERK and JNK MAP kinases. J. Biol. Chem. **282:**37412–37419.
45. **Wu, R. F., Y. C. Xu, Z. Ma, F. E. Nwariaku, G. A. Sarosi, Jr., and L. S. Terada.** 2005. Subcellular targeting of oxidants during endothelial cell migration. J. Cell Biol. **171**:893–904.
46. **Xiao, H., C. Neuveut, H. L. Tiffany, M. Benkirane, E. A. Rich, P. M. Murphy, and K. T. Jeang.** 2000. Selective CXCR4 antagonism by Tat: implications for in vivo expansion of coreceptor use by HIV-1. Proc. Natl. Acad. Sci. U. S. A. **97:**11466–11471.
47. **Yorimitsu, T., U. Nair, Z. Yang, and D. J. Klionsky.** 2006. Endoplasmic reticulum stress triggers autophagy. J. Biol. Chem. **281:**30299–30304.